

Optimization of protein patterns for neuronal cell culture applications

William M. Theilacker^{a)}

Department of Strategy and Scientific Operations, Medtronic, Inc., Minneapolis, Minnesota 55432-5604

Holt Bui and Thomas P. Beebe, Jr.

Department of Chemistry and Biochemistry, University of Delaware, Newark, Delaware 19716

(Received 4 April 2011; accepted 20 July 2011; published 22 August 2011)

In the present study, we fabricated two-component extracellular matrix protein patterned substrates with fibronectin (FN) and laminin (LN) because of our interest in the mechanism of axonal regeneration and injury in the central and peripheral nervous systems. The authors investigated how the patterning order and method of attachment affected the spatial distribution and biological activity of the immobilized proteins. Micro-contact printing (μ CP) techniques in concert with reactive surface chemistry were used to modify glass substrates with one- and two-component films of FN and LN, including micrometer-scale patterns of FN and LN. The composition and spatial distributions of both proteins on the patterned surfaces were characterized by x ray photoelectron spectroscopy, epi-fluorescence microscopy, atomic force microscopy, and time-of-flight secondary-ion mass spectrometry. The authors also characterized the biological activity of the top-most protein layer in a two-layer protein system as well as the ability of the top-most protein layer to mask the biological activity of an underlying protein layer using a fluorescence-based enzyme-linked immunosorbent assay. The order of protein deposition significantly affected the relative biological activity of the upper-most and underlying immobilized proteins. As a result of these optimization studies, maximum biological activity per surface protein was achieved by first immobilizing FN from solution, followed by μ CP of LN on the FN. Addition of μ CP LN films was able to mask \sim 84% of the underlying FN activity, whereas μ CP FN films were only able to mask \sim 27% of the underlying LN activity. © 2011 American Vacuum Society. [DOI: 10.1116/1.3624584]

I. INTRODUCTION

Surfaces displaying patterned biomolecules are paramount in the development of advanced biosensors,^{1–3} biomaterials,^{4,5} microarrays,^{6,7} and lab-on-a-chip devices⁸ for medical, defense, and scientific applications. Surface patterning offers the opportunity to control the spatial distribution of proteins and tune cellular events including cell attachment,^{9–12} process outgrowth,^{13–15} and other important morphological changes to specific substrate regions. At present, there are a number of soft-lithographic techniques¹⁶ that can be utilized to pattern surfaces on the micrometer scale with polydimethylsiloxane (PDMS) devices including microfluidic networks (μ FN),¹⁷ plasma-initiated patterning (μ PIP),^{18,19} replica molding (REM),^{20,21} micro-molding in capillaries (MIMIC),²¹ and micro-contact printing (μ CP).^{20–23} Micro-contact printing stands out from the list because it is one of the most inexpensive and facile techniques for patterning of biomolecules. In previous studies, we have shown that μ CP can create micrometer to sub-micrometer scale surface patterns from a wide variety of *biomolecular inks*, including extracellular matrix (ECM) proteins, biotin, streptavidin, and immunoglobulins (IgG) on polymeric, metallic, and inorganic surfaces with high spatial resolution.^{14,24–26}

It is important during the substrate patterning process that the biological activity and spatial contrast of the immobilized biomolecules are properly preserved and not compromised. It

has been shown that the properties of the substrate material, including surface roughness, chemical functionality, wettability, and rigidity, as well as the properties of the biomolecules themselves, including size, charge, and structure, play a major role in the activity of the immobilized biomolecules.^{27–34} The sequence of biomolecule deposition onto native (e.g., elemental and oxide) and chemically modified surfaces (e.g., self-assembled monolayers) can be varied to create different patterning routes that result in nearly identical biomolecule spatial contrast when viewed from above but that display differences in their overall biological activity. For example, in one possible route, biomolecule A is μ CP directly onto the substrate followed by a backfilling step in which biomolecule B reacts with the unstamped substrate regions. In a second possible route, the substrate is initially coated (through reactive chemical attachment) with a uniform layer of biomolecule A followed by μ CP with biomolecule B. Depending on the biomolecules of interest, one patterning route may offer better biological activity than the other.

A recent study by Wang *et al.* compared the film thickness, enzymatic activity, and structural conformation of adsorbed and μ CP films of horseradish peroxidase on amino- and bovine serum albumin (BSA)-terminated substrates.³⁵ When normalized to total protein, the enzymatic activity was \sim 10-fold higher when HRP was μ CP onto BSA-terminated substrates than on amino-terminated substrates. Solution adsorption of HRP onto amino-terminated substrates resulted in good biological activity, whereas deposition of HRP by μ CP resulted in a \sim 70% to 80% reduction in biological activity. However,

^{a)}Electronic mail: billtheilacker@gmail.com

when HRP was μ CP onto a BSA-coated substrate, the biological activity of HRP increased ~ 10 -fold. By using attenuated total reflectance-infrared spectroscopy (ATR-IR), they discovered that the amide-I band shifted from $\sim 1650\text{ cm}^{-1}$ (α -helix, characteristic of HRP) to $\sim 1615\text{ cm}^{-1}$ (anti-parallel β -sheet) for the stamped HRP films on non-BSA-coated substrates. They concluded that the decrease in biological activity was the result of a denser protein film morphology that sterically blocked the enzyme's active sites.

Although the present work does not address the behavior of neuronal and glial cell attachment and outgrowth on these types of patterned substrates, our group, as well as others, is interested in ECM protein patterned surfaces for nerve-cell engineering applications, and we have studied outgrowth in the past.^{14,36,37} This study is part of a larger project aimed at understanding neuronal pathfinding dynamics on patterned biomaterials displaying two or more ECM proteins to modulate axonal growth. Allowing the axons to choose between *more permissive* and *less permissive* substrates may be a way to control the nerve's transition across an unfavorable boundary (e.g., the glial scar), which may be encountered by a regenerating neuron after a spinal cord injury (SCI).³⁸

We chose to pattern the two important ECM glycoproteins fibronectin (FN) and laminin (LN) that modulate neuronal growth. FN [molecular weight (MW) $\sim 440\text{ kDa}$] is a dimeric glycoprotein with a central arginine-glycine-aspartic acid (RGD) integrin-binding domain that promotes cellular adhesion.³⁹ LN (MW $\sim 900\text{ kDa}$) is a heterotrimeric glycoprotein with three polypeptide chains ($\alpha 1$, $\beta 1$, $\gamma 1$) that assemble into a three-stranded, coiled-coil, crosslike structure if confined to a single plane.⁴⁰ Polypeptide sequences within LN have been identified with specific biological activities including neural cell adhesion, cell migration, and neurite outgrowth.^{40–43}

We hypothesized that the sequence and method of biomolecule deposition in the preparation of ECM protein patterned surfaces may affect the spatial distribution and biological activity of fibronectin (FN) and laminin (LN). In this work, we created alternating $40\text{-}\mu\text{m}$ -wide lanes of FN and LN on cross-linker-modified glass substrates through a combination of micro-contact printing techniques and reactive surface chemistry. The substrate patterning sequence was investigated in an attempt to optimize the biological activity and spatial contrast of each patterned protein. Using fluorescently labeled proteins, we attempted to quantify the relative *protein contrast* for each patterned protein by fluorescence microscopy. A closer examination of the patterned substrates with surface-sensitive analytical techniques, including time-of-flight secondary-ion mass spectrometry (TOF-SIMS), x-ray photoelectron spectroscopy (XPS), and atomic force microscopy (AFM) provided spatial distribution, surface coverage, and surface texture information. To determine if the sequence of substrate patterning affected the biological activity of the substrate-bound ECM proteins, we developed a fluorescence-based enzyme-linked immunosorbent assay (ELISA). Mono- and dual-component ECM protein films were designed to mimic the patterned substrates and were reacted with epitope-specific monoclonal antibodies toward FN and LN

that are known to influence neuronal cell adhesion and neurite outgrowth. In addition, we compared the long-term interfacial stability of the immobilized protein layers.

II. EXPERIMENTAL SECTION

A. Materials

Water was deionized, distilled over quartz and filtered by a Milli-Q reagent water system (Millipore Co.), which resulted in a resistivity of $18\text{ M}\Omega \times \text{cm}$.

B. Chemically modified glass cover slips

Glass cover slips were chemically functionalized through a three-step process to generate a succinimide-ester terminated surface that was reactive toward primary amines on proteins and peptides. The reaction scheme is shown in Fig. 1. Prior to silanization, glass cover slips (12 mm, No. 2, Fisher Scientific) were cleaned in piranha solution [7:3 (v/v) $\text{H}_2\text{SO}_4/\text{H}_2\text{O}_2$] for 30 min. Great caution and the proper personal protective equipment were used with this highly acidic and highly oxidizing solution. The cover slips were then thoroughly rinsed with water, followed by ultrasonic cleaning in water for 30 min. The cleaned cover slips were then dried with a gentle stream of nitrogen, covered with aluminum foil, and further dried on a hotplate at 150°C for approximately 1 h. The piranha-cleaned cover slips were immediately transferred into an inert atmosphere (N_2 glovebag) and immersed in a 2% solution (by weight) of 3-mercaptopropyl trimethoxysilane (MTS, Sigma Aldrich) in dry toluene (Sigma Aldrich) for 2 h. The thiol-terminated glass cover slips were removed from the MTS solution, thoroughly rinsed with dry toluene, then with absolute ethanol (Fisher Scientific), and finally dried with a gentle stream of nitrogen. The cover slips were covered with aluminum foil and thermally cured at 70°C for 1 h outside of the N_2 glovebag.

The heterobifunctional cross-linker, *N*- γ -maleimidobutylsuccinimide ester (GMBS, Sigma Aldrich) was dissolved in a minimum volume ($\sim 1\%$ by volume) of dimethylformamide (Sigma Aldrich) and diluted to volume with absolute ethanol to yield a final concentration of 2 mM. The cover slips were immersed in this GMBS solution for 1 h, then thoroughly rinsed $3 \times$ with absolute ethanol and dried with a gentle stream of nitrogen. We previously reported the surface characterization of each chemical reaction step by contact angle, XPS, and TOF-SIMS.¹⁴

C. Labeling fibronectin and laminin with fluorescent dye

Bovine plasma FN (Calbiochem) and Engelbreth-Holm-Swarm murine LN (Chemicon) were fluorescently labeled with protein labeling kits from Invitrogen (Life Technologies) and diluted to a final concentration of $50\text{ }\mu\text{g/ml}$ in Dulbecco's phosphate buffered saline (PBS, $\text{pH} \sim 7.4$, Fisher Scientific). The protein FN was labeled with Alexa Fluor-633, and the protein LN was labeled with Oregon Green 488. The degree of protein labeling was determined by UV-visible spectroscopy (UV-vis Chemstation, Agilent Technologies, Santa

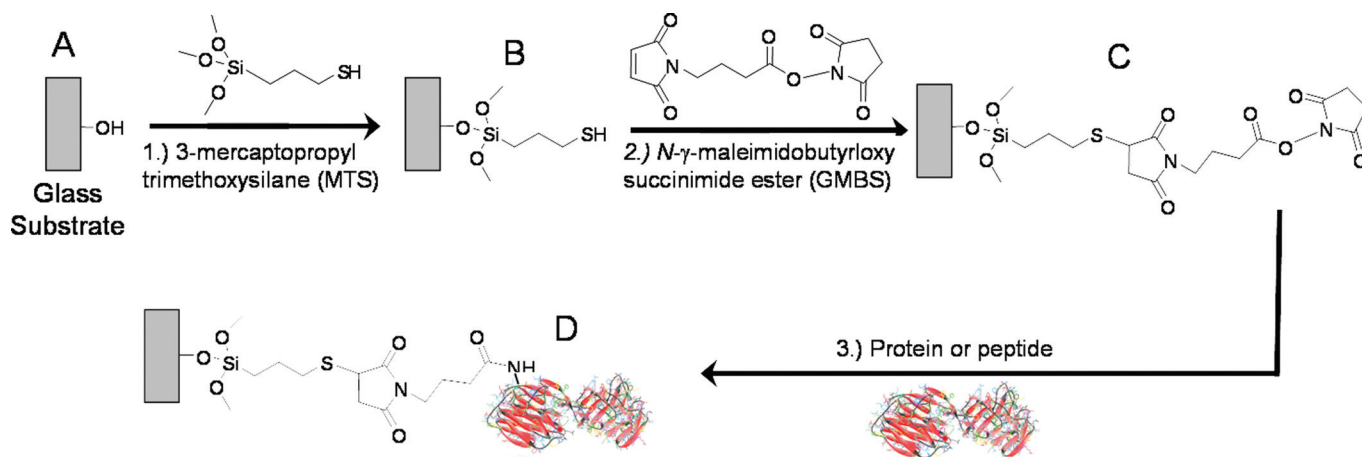


Fig. 1. (Color) Schematic diagram of surface chemistry reaction steps used to create functionalized surfaces for the covalent immobilization of proteins and peptides. A piranha-cleaned glass substrate bearing hydroxyl groups (a) is reacted with 3-mercaptopropyl trimethoxysilane (3-MTS) to produce a thiol-terminated surface (b). The heterobifunctional cross-linker *N*- γ -maleimidobutyryloxy succinimide ester (GMBS) is reacted with the thiol-terminated surface (b) to create a surface (c) that is reactive with primary amine groups, such as from a protein, peptide, or other species.

Clara, CA) following the procedure provided with the labeling kit. Approximately 7 molecules of Alexa Fluor 633 dye were conjugated per molecule of FN and ~ 12 molecules of Oregon Green dye were conjugated per molecule of LN.

D. Preparation of dual ECM-protein patterns on GMBS-modified substrates

Micro-contact printing and reactive surface chemistries were used to create dual-ECM protein patterns on GMBS-modified substrates. The protein patterning scheme is outlined in Fig. 2(a) to produce alternating $40\text{-}\mu\text{m}$ -wide lanes of FN and LN over a 1-cm^2 region. GMBS-modified substrates were immersed in the first protein solution consisting of $50\text{-}\mu\text{g/ml}$ LN (Oregon Green 488) for 2 h at 4°C . The substrates were rinsed with Tween-20 (0.05% by volume, Sigma Aldrich) in PBS (herein referred to as PBS-T) for 30 min. Prior to micro-contact printing the second protein, the LN-coated substrates were dried under a gentle stream of N_2 . Patterned PDMS stamps were inked with $50\text{-}\mu\text{g/ml}$ FN (Alexa Fluor 633) in PBS and incubated for 30 min at 4°C . The PDMS stamps were briefly rinsed with PBS and water to remove excess FN and dried under a gentle stream of N_2 . The PDMS stamps were immediately brought into conformal contact with the LN-coated substrates with a normalized force of $200\text{ g}\cdot\text{cm}^{-2}$ for 30 min at 37°C . After stamping, the substrates were rinsed with either PBS or PBS-T for 30 min and stored at 4°C until analysis.

E. Preparation of mono- and dual-component ECM-protein films on GMBS-modified substrates

The preparation of mono- and dual-component protein films of FN and LN (nonfluorescently labeled) is shown schematically in Fig. 2(b). GMBS-modified cover slips were immersed in $50\text{-}\mu\text{g/ml}$ FN or LN (substrates 1 and 3) solutions prepared in PBS at $\text{pH} \sim 7.4$ for 2 h and subsequently rinsed with PBS-T to remove noncovalently attached protein. Prior

to micro-contact printing of the second protein layer (substrates 2 and 4), the substrates were rinsed with water and dried under a gentle stream of N_2 . PDMS stamps presenting a flat printing surface (featureless) were inked with $50\text{-}\mu\text{g/ml}$ FN or LN and incubated for 30 min at 4°C . The surface area of the printing face for each PDMS stamp was greater than the diameter of the circular cover slips to ensure uniformly distributed protein coverages across the entirety of each substrate. PDMS stamps were rinsed with PBS and water to remove all but a thin film of adsorbed protein and dried under a gentle stream of N_2 . The PDMS stamps were immediately brought into conformal contact with the protein-coated substrates or GMBS-only substrates (substrates 5 and 6) with a normalized force of $200\text{ g}\cdot\text{cm}^{-2}$ for 30 min at 37°C . The slides were rinsed with PBS-T for 30 min and stored in PBS at 4°C until ELISA analysis. The sample preparation scheme outline in Fig. 2(b) produces a set of mono- and dual-component protein films with variation of the order of stamping, the order of reaction with a covalent cross-linker, and the degree of coverage of one protein by another.

F. Determination of biological activity of substrate-bound ECM-protein films

Mono- and dual-component ECM-protein films of FN and LN were blocked with 5% goat serum (GS, Chemicon) and 1% BSA (Sigma) in PBS for 2 h at 4°C and then rinsed $3\times$ with PBS. The substrates were immersed in primary antibody solutions specific to FN (mouse mAb, clone 17, Abcam, 1:250 dilution) and LN (rat mAb, clone AL-4, Chemicon, 1:250 dilution) for 2 h at RT. The substrates were rinsed with PBS-T for 30 min followed by PBS. Secondary antibodies consisting of horseradish peroxidase (HRP)-conjugated goat anti-rat and goat anti-mouse immunoglobulins (Jackson ImmunoResearch Laboratories) were diluted 1:101000 in 5% GS. The substrates were immersed for 3 h at RT and thoroughly rinsed with PBS-T followed by PBS.

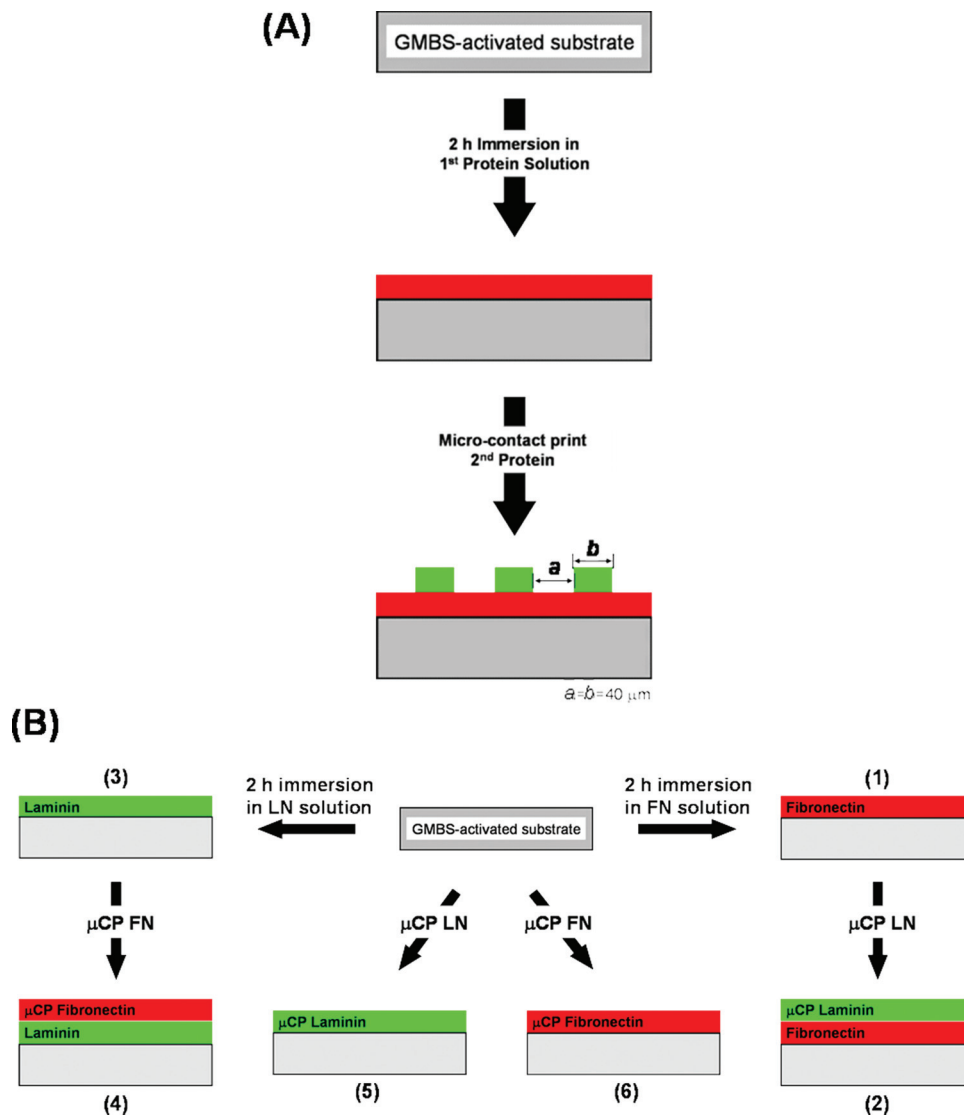


FIG. 2. (Color) Surface modification schemes utilizing micro-contact printing and reactive surface chemistries to produce (a) dual-ECM protein patterns and (b) mono- and dual-component unpatterned protein films.

The substrates were dried with N₂ and transferred to a multiwell sample plate prior to adding 100-μM Amplex[®] Red reagent (10-acetyl-3,7-dihydroxyphenoxazine) and 20-mM H₂O₂ (Amplex Red assay kit, Invitrogen) prepared in sodium phosphate buffer (0.05 M, pH ~ 7.4) to each sample well. The enzymatic reaction was allowed to proceed for 30 min at RT while protected from light. Three separate 100-μl aliquots were taken from each sample well and transferred to a black 96-well assay plate with a clear glass bottom (Corning, Inc.). The fluorescence intensity was measured using a PerkinElmer[™] Fusion Universal Microplate Analyzer (Waltham, MA) with a 535 ± 25 nm excitation filter and a 590 ± 10 nm emission filter. The enzymatic activity of HRP was correlated to the biological activity of substrate-bound protein epitopes following normalization to the relative amount of protein on the surface by XPS analysis. A minimum of three test samples (n = 3) were analyzed for each protein-modified substrate.

G. Atomic force microscopy (AFM)

The surface topography of the micro-contact printed FN and LN films were imaged by intermittent-contact AFM (also known as tapping-mode) in air on a Bioscope scanning probe microscope (Digital Instruments, Veeco Metrology Group, Chadds Ford, PA) mounted on a TE-2000-S inverted fluorescence microscope (Nikon Instruments, Inc., Melville, NY). Budget Sensors Multi75A1 silicon AFM probes with a low force constant (~3 N/m) and a moderate resonance frequency (~75 kHz) were used to collect height and phase images. Protein film thickness values were calculated from a series of line profiles drawn perpendicular to the stamped protein-GMBS interface from 1 μm² AFM images with 1024 × 4096 pixel density.

H. X-ray photoelectron spectroscopy (XPS)

XPS analysis was performed on an Escalab 250i-XL electron spectrometer (VG Scientific, UK) with a monochromatic

Al K α (1486.6 eV) X-ray source. Measurements were carried out using a take-off angle of 90° with respect to the sample surface. The analyzed area was an elliptical spot of $\sim 400 \mu\text{m}$ diameter having an approximately Gaussian edge and flat-topped intensity profile. Survey scans over a binding energy range of 0–1200 eV were acquired for each sample with a constant analyzer pass energy of 100 eV at a data spacing of 1 eV $^{-1}$, followed by high-resolution spectra with a constant analyzer pass energy of 20 eV at a data spacing of 0.1 eV $^{-1}$. High-resolution spectra were used for quantitative determination of binding energies and atomic percentages. Depending upon sample conditions and S/N , spectra were signal averaged for ≥ 15 scans in each spectral range. Sample charging was compensated by use of a low-energy electron flood gun, typically operated at 6.0 eV. All peaks were shifted so that the methylene component of the carbon 1s envelope was centered at 284.6 eV. Shirley background subtraction, peak fitting and quantitation were performed with CASAXPS v2.2.24 software (Casa Software Ltd., UK).

I. Time-of-flight secondary-ion mass spectrometry (TOF-SIMS)

Static TOF-SIMS imaging was performed on a TOF-SIMS IV instrument (ION-TOF, Münster, Germany) using a 25-keV monoisotopic $^{69}\text{Ga}^+$ primary ion beam generated by a Ga^+ ion gun. High mass resolution (up to $m/\Delta m = 101000$ at $m/z = 28$) was obtained using “bunched mode” of the TOF-SIMS instrument. The typical target current of the primary Ga^+ beam in bunched mode was ~ 1 pA with a prebunched pulse width of 25 ns. Following bunching, the arrival pulse width, as judged by FWHM of the H^+ peak, was typically less than 700 ps. For imaging applications, the raster area of the Ga^+ ion beam was $400 \times 400 \mu\text{m}^2$ with a pixel density of 128×128 to attempt to match the pixel size with the Ga^+ ion beam spot size ($\sim 3 \mu\text{m}$ diameter). Low-energy electrons (20 eV) were supplied by a pulsed electron flood gun for charge compensation. All primary Ga^+ ion fluences were below the threshold (1×10^{12} ions $\cdot \text{cm}^{-2}$) for static SIMS. Both positive- and negative-ion images were acquired.

J. Sessile drop goniometer

Static contact angle measurements were acquired using an FTA125 sessile drop goniometer (First Ten Ångströms, Portsmouth, VA) with an RS170 camera. Aliquots (4- μl) of ultra-pure water were robotically pipetted onto the functionalized surfaces. Using a microscopic profile view of the sessile drop, contact angles were measured and calculated using an automated fitting program and FTA32 v2.0 software as previously described.¹⁴

K. Fluorescence microscopy

Dual ECM-protein patterned substrates were imaged using a TE-2000-S inverted fluorescence microscope (Nikon Corp., Melville, NY) with $10 \times$ (numerical aperture value of 0.30) and $20 \times$ (numerical aperture value of 0.45) Plan-Fluor

objectives, motorized sample stage and a mercury excitation source. The microscope was outfitted with a CoolSNAP-Pro CCD camera (Roper Scientific Photometrics, Trenton, NJ), and images were captured with IMAGE PRO EXPRESS 4.5 software (Media Cybernetics). Fluorescence images were collected from each filter channel (green channel: $\lambda_{\text{excitation}} 480 \pm 15$ nm, $\lambda_{\text{emission}} 535 \pm 20$ nm; and red channel: $\lambda_{\text{excitation}} 560 \pm 20$ nm, $\lambda_{\text{emission}} 630 \pm 30$ nm) and merged together in IMAGEPRO EXPRESS.

III. RESULTS AND DISCUSSION

A. Fluorescence imaging of FN and LN dual patterns

Dual-ECM protein patterns on GMBS-modified substrates were prepared with Oregon Green 488-conjugated LN in some areas and Alexa Fluor 633-conjugated FN in other areas and imaged by fluorescence microscopy. A representative fluorescence image of a FN/LN patterned substrate is shown in Fig. 3(a). The patterning scheme produced good spatial contrast of alternating 40- μm -wide lanes of FN and LN. For each acquired fluorescence image, a line profile (white line across fluorescence image, Fig. 3(a)) was drawn perpendicular to the lane direction of the striped protein pattern to measure the pixel intensities as shown in Fig. 3(b). It can clearly be seen that for both the red channel (FN) and the green channel (LN) of images collected at the same location, under the same conditions, fluorescent intensity is at a maximum for one protein where it is at a minimum for the other over the ~ 10 pairs of FN/LN lanes shown.

To make maximal use of all data contained within each image, the images were further quantified by generating image intensity histograms for each fluorescence wavelength channel according to our previously published results.²⁴ Two well resolved peaks were generally observed in such histograms: one centered at the background intensity ($I_{\text{background}}$), and one centered at the labeled protein intensity (I_{protein}). In an attempt to quantify image contrast, the intensity of the background fluorescence centroid and labeled protein fluorescence centroid were determined by fitting the peaks to a two-component Gaussian distribution in ORIGIN (Version 7.5 SR6, OriginLab Corporation). The results of such an analysis are shown in Fig. 3(c). We define the relative *protein contrast* for FN and LN by the ratio ($I_{\text{protein}}/I_{\text{background}}$). This ratio is a helpful metric to evaluate the interfacial stability of patterned protein layers on test substrates such as these and others.

The interfacial stability of the immobilized protein layers was probed with respect to various rinsing steps using the nonionic surfactant Tween-20. Tween has been shown to reduce nonspecific protein adsorption and hydrophobic interactions on silicon-based surfaces.⁴⁴ After patterning, the substrates were rinsed with either PBS or PBS-T for 30 min prior to fluorescence imaging. The results are shown in Fig. 3(d). Protein contrast ratios for FN and LN before and after PBS-T rinsing were compared using a pairwise *t*-test at the 95% confidence level. LN that was covalently immobilized from solution onto GMBS-modified substrates exhibited no significant change in protein contrast after rinsing ($P = 0.8$), whereas the

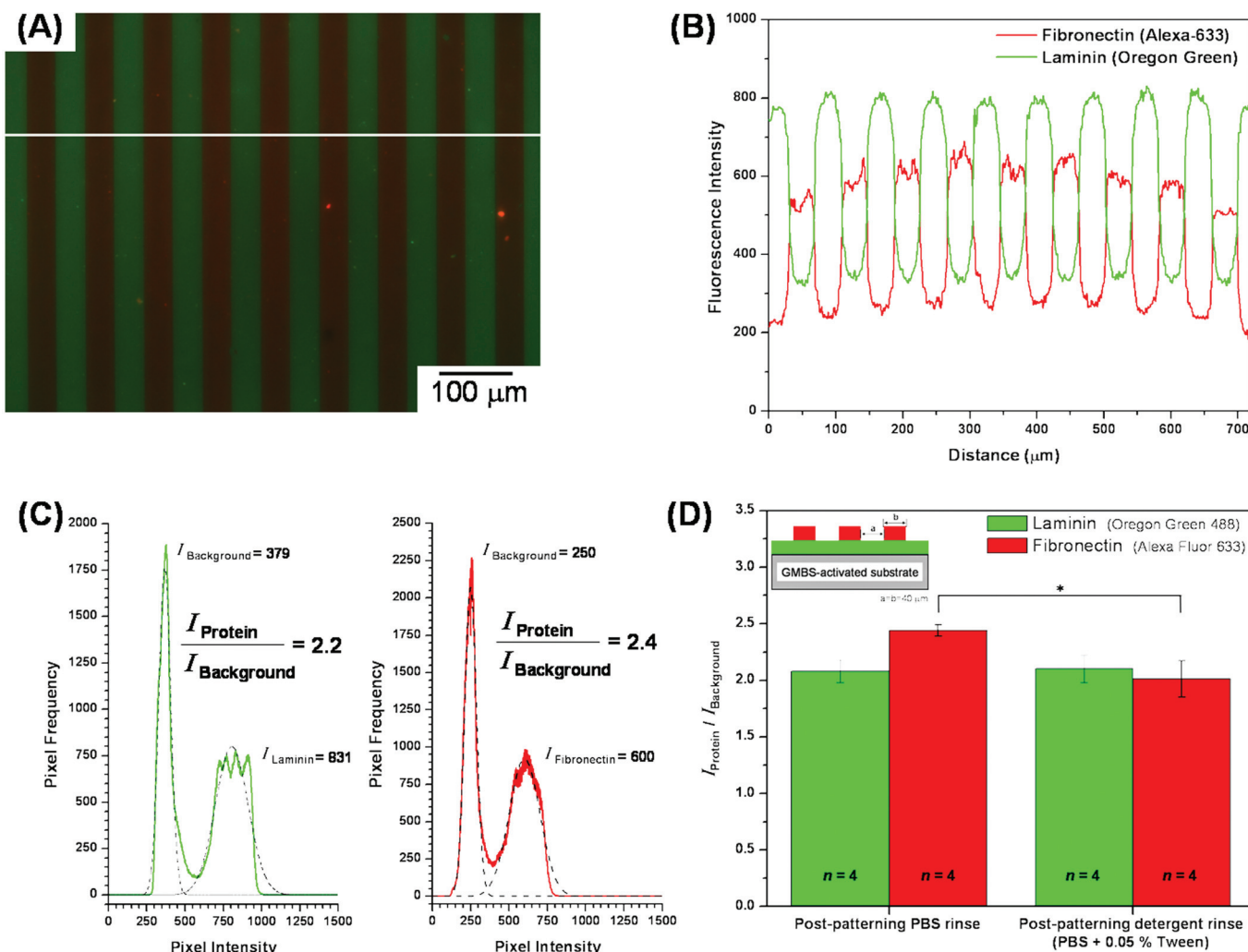


FIG. 3. (Color) Fluorescence imaging and image processing of dual-ECM protein-patterned substrates. (a) Representative fluorescence image of a FN/LN dual pattern (with post-patterning PBS rinse) prepared on a GMBS-modified substrate by micro-contact printing and reactive surface chemistry. 40- μm -wide lanes of FN are shown in red and 40- μm -wide lanes of LN are shown in green. (b) A line profile was drawn perpendicular to the pattern orientation as indicated by the horizontal white line in (a), showing the pixel intensities, for both the red and green channels, across the substrate. (c) Image intensity histograms of the green channel (LN, left) and red channel (FN, right) were generated to show the distribution of pixel intensities contained within the entire sample image. In an attempt to quantify image contrast, pixel intensities were fitted to a Gaussian distribution (black dotted lines) representing a two-component system, $I_{\text{background}}$ and I_{protein} . The relative “protein contrast” for FN and LN is defined as the ratio ($I_{\text{protein}}/I_{\text{background}}$). (d) The effect of detergent rinsing on the relative FN and LN contrast. After protein patterning, the substrates were rinsed with either PBS or PBS-T (PBS containing 0.05% Tween-20) for 30 min to determine the interfacial stability of both the covalently attached LN layer and the micro-contact-printed FN lanes on the LN-coated substrate. Data reported as means \pm standard deviation. The sample means were compared by a pairwise *t*-test. *Sample means statistically different at the 95% confidence level.

protein contrast ratio in the stamped FN regions decreased $\sim 18\%$ (statistically significant) after rinsing with PBS-T ($P = 0.007$).

B. TOF-SIMS imaging of dual-ECM protein patterned substrates

TOF-SIMS imaging was performed to provide long-range molecular information about the spatial distribution of the patterned ECM proteins from the top-most surface regions ($\sim 1\text{--}2$ nm). Mass-resolved positive- and negative-ion images provided good spatial resolution of the alternating 40- μm -wide protein lanes as shown in Fig. 4 for both positive ions (a) and negative ions (b). The LN regions that were not over-stamped with FN exhibited the highest pixel intensities for both

protein- and substrate-specific fragment ions. For example, the low-molecular-weight hydrocarbon ion C_2H_3^+ ($m/z = 27.023$), a common fragment ion for both proteins and the underlying GMBS-substrate chemistry, showed a higher pixel intensity in the nonstamped LN regions than in the over-stamped FN regions. A similar trend was observed for higher mass-to-charge hydrocarbon species (images not shown) as well as for fragment ions that principally originate from the glass substrate (O^- , $m/z = 15.995$ and OH^- , $m/z = 17.003$). Fragment ions indicative of the protein backbone (CN^- , $m/z = 26.003$ and CNO^- , $m/z = 41.998$) were also observed. The immonium ions for glycine (CH_4N^+ , $m/z = 30.034$) and lysine ($\text{C}_2\text{H}_6\text{N}^+$, $m/z = 44.050$) were selected to represent, respectively, an amino acid that was *similar* in bulk concentration and one that

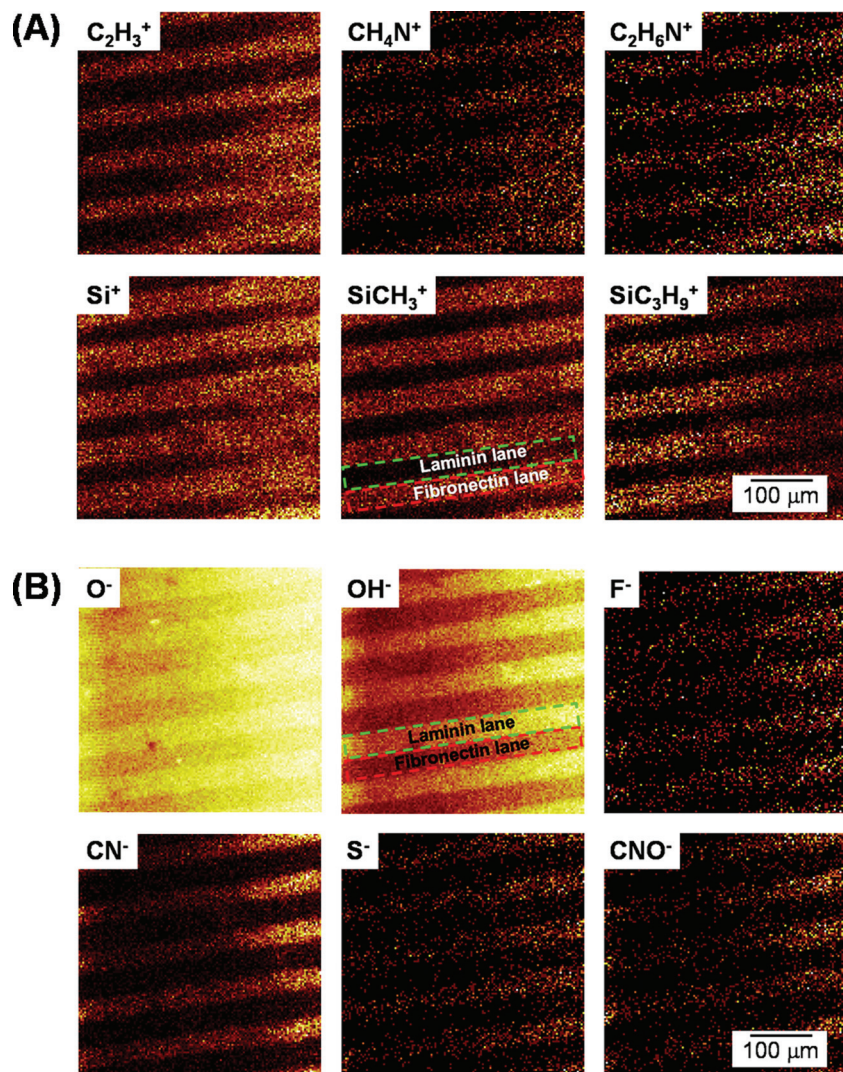


FIG. 4. (Color) TOF-SIMS images of dual-ECM protein patterns consisting of alternating 40-mm-wide lanes of FN and LN prepared on GMBS-modified substrates with fluorescently labeled protein (used in parallel experiments for fluorescence microscopy). Mass-resolved positive-ion (a) and negative-ion (b) images of representative protein- and substrate-related fragment-ions were normalized to the total-ion intensity. A label indicating the spatial orientation of the two proteins is shown in the SiCH_3^+ image for positive-mode imaging and in the OH^- image for negative-mode imaging. The transfer of PDMS oligomers to the protein-modified substrates during the micro-contact printing step was confirmed by high SiCH_3^+ and SiC_3H_9^+ ion-intensities only in the stamped regions (*i.e.*, FN here). These fragments are particularly stable, giving perhaps an inflated impression of PDMS contamination in stamped protein lanes. For example, other non-PDMS fragments can also be seen in stamped lanes (e.g., C_2H_3^+ , CH_4N^+ , $\text{C}_2\text{H}_6\text{N}^+$), although not as intense as in nonstamped lanes.

was substantially *different* in bulk concentration for LN versus FN (see Supplemental Table 1).^{45,46} Glycine's amino acid count was only $\sim 2.0\%$ different for FN versus LN (both around 8.1% of amino acid residues), whereas lysine's amino acid count differed by $\sim 29.7\%$ for FN versus LN (3.4% for FN versus 4.8% for LN). For both immonium-ions, higher pixel intensities were observed on the nonstamped LN regions than on the FN over-stamped regions. Despite the substantial difference (34.9%) in lysine amino acid residues for the bulk LN and FN proteins, the immonium ion originating from lysine ($\text{C}_2\text{H}_6\text{N}^+$, $m/z = 44.050$) exhibited a LN-to-FN image contrast of ~ 3.3 in this ion's TOF-SIMS image. The immonium ion image resulting from glycine (CH_4N^+ , $m/z = 30.034$) exhibited a LN-to-FN image contrast of ~ 6.7 in this ion's TOF-SIMS image. Thus, the TOF-SIMS *protein contrast* exceeded the bulk protein composition ratios for two example

amino acids, glycine and lysine. TOF-SIMS imaging was also able to detect a weak spatial distribution of fluoride ions (F^-), which resided only in the LN regions because each molecule of Oregon Green 488 contained two atoms of fluorine, and each LN protein was labeled with ~ 12 Oregon Green 488 molecules.

The lower pixel intensity of protein- and substrate-related fragment ions in the stamped FN regions may be due to the presence of low-molecular-weight silicone contamination (PDMS oil). Low-molecular-weight PDMS oligomers were observed on the stamped FN regions as a result of the micro-contact printing process. This was confirmed by the image contrast observed for the Si^+ ($m/z = 27.977$), SiCH_3^+ ($m/z = 43.000$), and SiC_3H_9^+ ($m/z = 73.047$) ion images, which showed a higher intensity in the stamped FN regions than in the unstamped LN regions. These $[\text{Si}(\text{CH}_3)_n]^+$ ions (and

others not shown here) are signature fragments of PDMS and are particularly abundant and stable, giving perhaps, an exaggerated impression of PDMS contamination.^{47,48} Other ions indicative of PDMS were also observed (data not shown) in the FN regions.

C. Biological activity of FN and LN as a function of protein immobilization on GMBS-modified substrates

The order and route of FN and LN reaction or deposition (*i.e.*, covalent attachment from solution, covalent attachment after stamping, stamping on top of another protein) on GMBS-modified substrates was investigated to determine if the patterning sequence affected the biological activity of specific protein domains known to influence neuronal cell adhesion and neurite outgrowth. An ELISA assay was used to measure the biological activity per surface protein as shown in Fig. 5. For the FN part of this assay, we used the FN monoclonal antibody A17, which has a high affinity for the 120-kDa cell-binding domain that encompasses the central

RGD integrin-binding motif and the PHSRN site. For the LN part of this assay, we used the LN monoclonal antibody AL-4, which has a high affinity for the LN $\beta 1$ and/or $\gamma 1$ coiled-coil domains.^{49,50} Substrates were prepared as uniform (*i.e.*, non-patterned) protein films consisting of mono- or dual-component protein films using featureless rather than patterned PDMS stamps. This was done to ensure that the total stamped area was constant, thereby normalizing the assay intensity per unit area for all samples. For each protein-modified substrate, the enzymatic activity of HRP was normalized to the amount of substrate-bound protein, as determined by XPS analysis, and as shown in Supplemental Fig. 1.⁴⁶ The XPS atomic percentage (at. %) ratios of nitrogen (N 1s) to silicon (Si 2p) from each substrate were used to quantify the relative protein surface coverages of FN and LN.

The biological activity per FN or LN surface protein was dependent upon the protein deposition method as shown in Fig. 6. The biological activity of the FN domain that is reactive toward the FN A17 antibody, as judged by the normalized HRP activity, was greatest when FN was immobilized

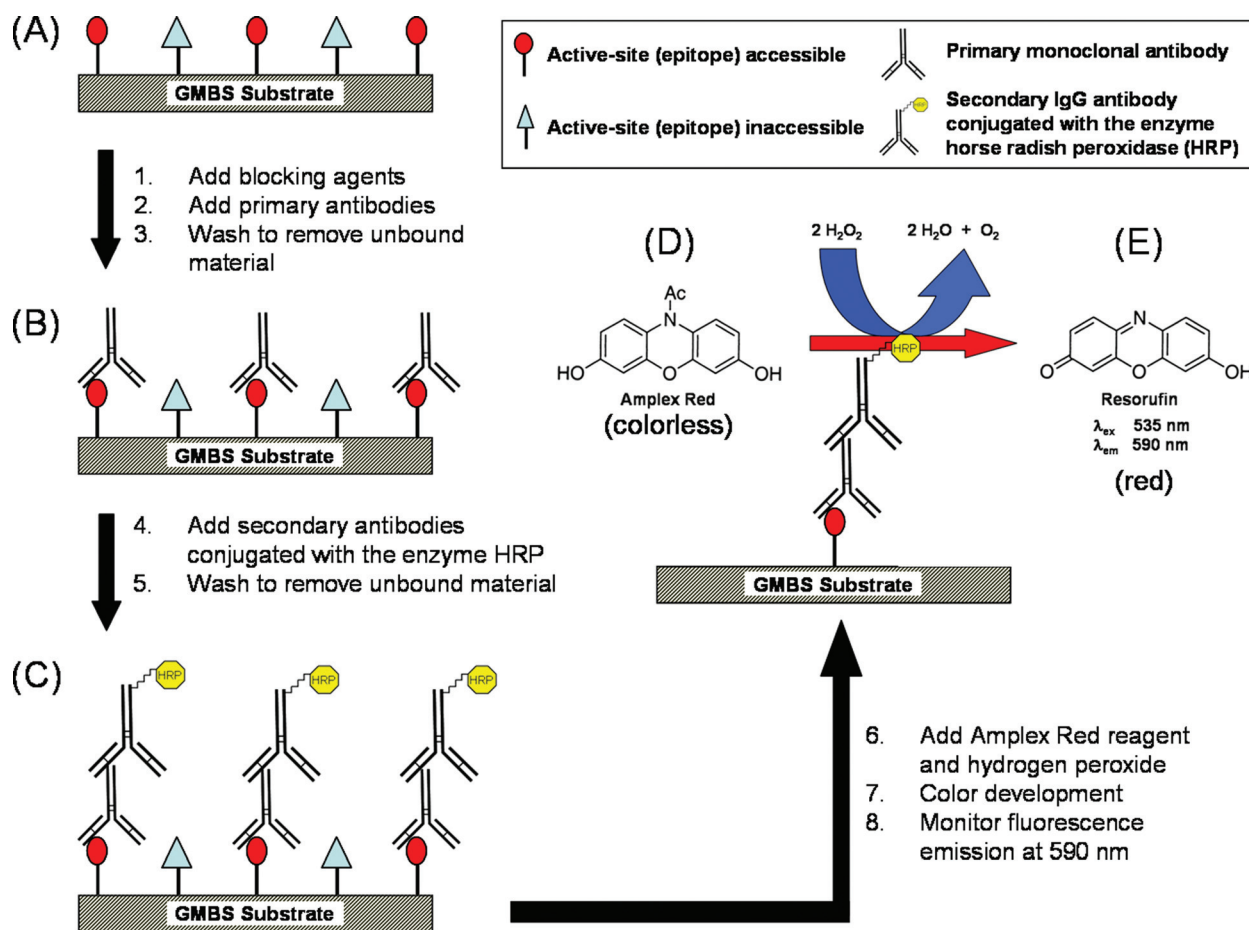


Fig. 5. (Color) Determination of biological activity per surface protein with a fluorescence-based ELISA assay. The implicit assumption for this assay is that the binding of the primary antibodies in step A→B can only occur when the target epitope in LN or FN is present and accessible (*i.e.*, “biologically active”). Mono- and dual-component ECM protein films [substrates 1 through 6 as shown in Fig. 2(b)] (a) were reacted with structurally specific mAb towards FN (clone A-17) and LN (clone AL-4) (b) and subsequently reacted with horseradish peroxidase (HRP)-conjugated secondary IgGs (c). The reduction of hydrogen peroxide by HRP resulted in the oxidation of Amplex red (colorless, d) to form a red fluorescent product (resorufin, e). The magnitude of the normalized fluorescence intensity was correlated to the HRP activity of substrate-bound FN and LN protein active sites (epitopes) known to influence cell adhesion and neurite outgrowth.

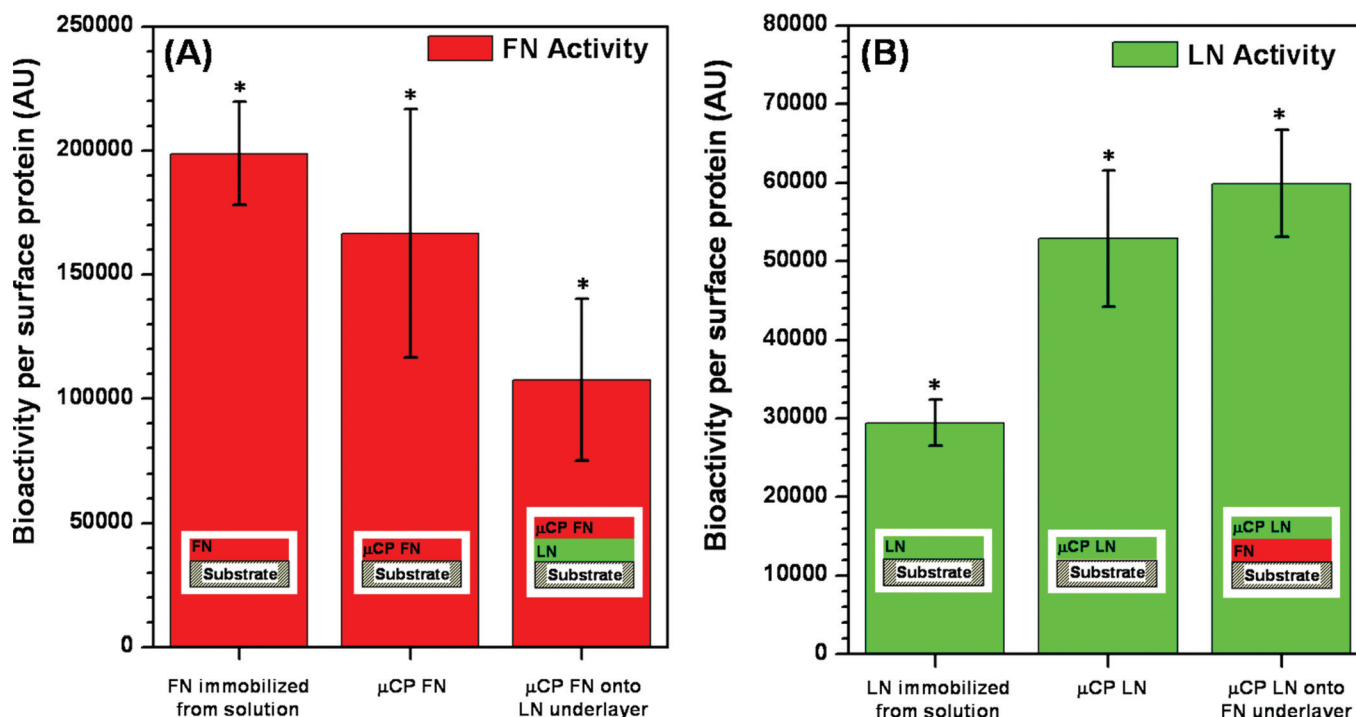


FIG. 6. (Color) Using the ELISA assay in Fig. 5, we determined FN (a) and LN (b) biological activity after reaction with GMBS-modified substrates as a function of the method (*i.e.*, covalent attachment from solution, covalent attachment after stamping, stamping on top of another protein) of protein deposition. The direct activity of the top-most protein in cases (1) through (6) of Fig. 2(b) were tested here. Bioactivity per surface protein was assayed by a fluorescence-based ELISA using epitope-specific primary mAb toward FN (clone A-17) and LN (clone AL-4) with HRP-conjugated secondary IgGs (see Fig. 5). Test substrates were prepared as either mono- or dual-component protein films consisting of uniform surface coverages with no spatial patterning. Featureless PDMS stamps were used to μ CP FN and LN films. The HRP activity of each protein-modified substrate was normalized to the relative amount of surface-bound protein determined by XPS analysis (see Supplemental Fig. 1). HRP bioactivity per surface protein is reported as mean \pm standard deviation ($n = 12$). The substrates were compared by a one-way ANOVA at the 95% confidence level, and each protein deposition route resulted in a statistically different response in FN and LN bioactivity ($P < 0.001$). *Denotes that the FN and LN bioactivity was statistically different from the indicated protein deposition routes ($P < 0.001$); for the comparison between μ CP LN films on both a GMBS-modified substrate (b, center) and on a FN-coated substrate (b, right), $P = 0.04$. Cross-reactivity control experiments are shown in Fig. 7.

from solution onto a GMBS-modified surface (substrate 1, see Figs. 2(b) and 6(a)). μ CP FN showed a reduction in HRP activity and was dependent on the underlying substrate chemistry. The biological activity per FN surface protein decreased by $\sim 16\%$ when FN was stamped directly onto a GMBS-modified surface (Fig. 2(b), substrate 6) and by $\sim 46\%$ when stamped onto a LN-coated surface (Fig. 2(b), substrate 4). These three FN deposition routes were statistically different from each other ($P < 0.001$, t -test, pairwise comparisons).

For LN, the opposite trend in biological activity was observed. The biological activity of the LN was greatest when LN was μ CP onto a FN-coated surface (Fig. 2(b), substrate 2). The biological activity per LN surface protein decreased by $\sim 12\%$ when LN was μ CP directly onto a GMBS-modified surface (Fig. 2(b), substrate 5) and by $\sim 51\%$ when LN was immobilized from solution onto a GMBS-modified surface (Fig. 2(b), substrate 3). All three LN immobilization routes were statistically different from each other ($P < 0.001$, t -test, pairwise comparisons) except for the comparison between LN stamped directly onto a GMBS-modified surface and LN stamped onto a FN-coated surface ($P < 0.04$).

The interfacial stability of the protein films was probed with the detergent Tween-20 in PBS. substrates 1–6

(Fig. 2(b)) exhibited a reduction in biological activity per surface protein ranging from $\sim 3\%$ to 15% (rinsed with PBS-T for 30 min) when in comparison to the substrates rinsed only with PBS. These results are in good agreement with the $\sim 18\%$ reduction in the relative FN contrast by fluorescence microscopy as shown earlier in Fig. 3(d). Even though we observed a significant decrease in the protein contrast ratio for FN after detergent rinsing, the stamped FN lanes adhered very well to the LN-coated substrates. The favorable interfacial bonding between FN and LN can be attributed to strong intermolecular forces, including hydrophobic and electrostatic interactions. For example, electrostatic interactions between FN and LN may play a significant role due to the difference in their isoelectric points (FN pI ~ 5.6 – 6.1 and LN pI ~ 5.0).^{29,51}

An important metric for the preparation of multiprotein patterned substrates is the ability of the topmost protein layer(s) to mask the biological availability of the underlying protein layer(s) on which they reside. Here we measured the biological activity of FN (Fig. 2(b), substrate 2: μ CP LN on a uniform FN layer) and LN (Fig. 2(b), substrate 4: μ CP FN on a uniform LN layer) with primary monoclonal antibodies (mAb) that were specific toward the *underlying* protein layer. The biological activity per surface protein of the

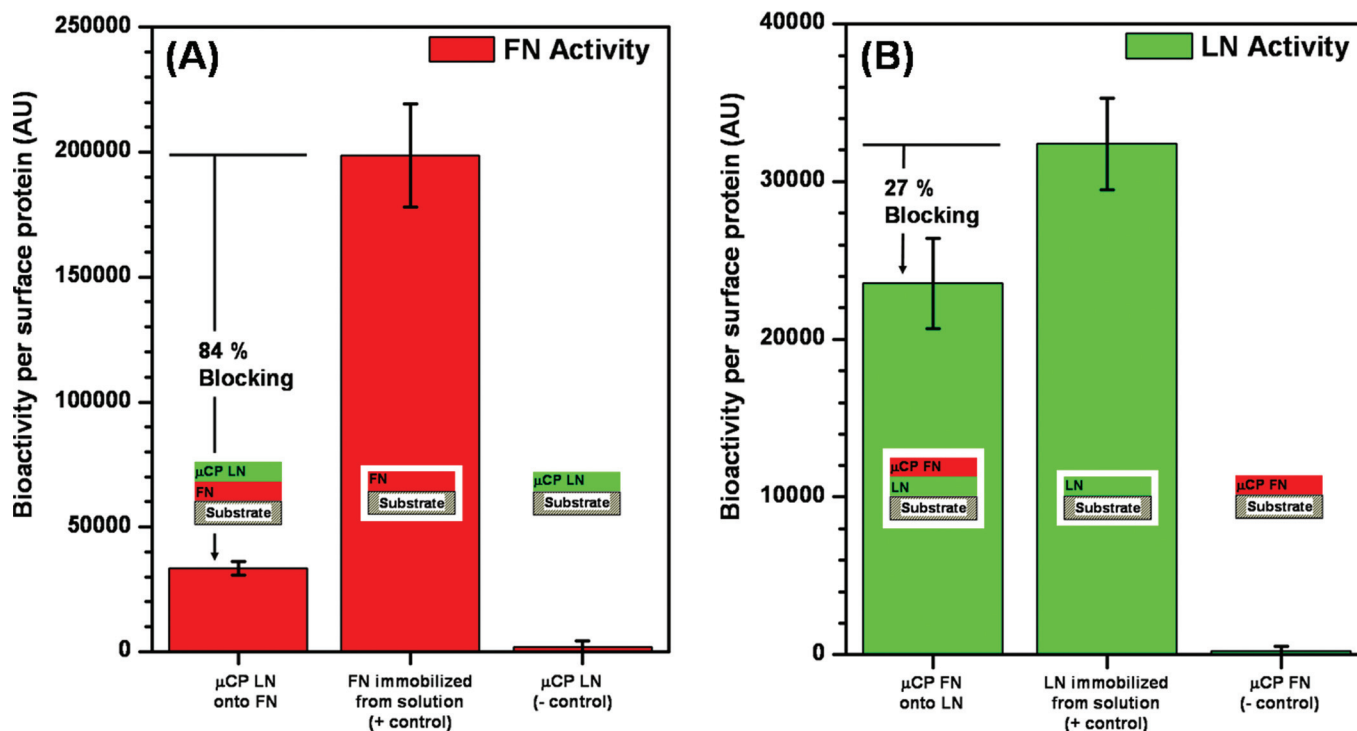


Fig. 7. (Color) Using the ELISA assay in Fig. 5, we determined the ability of the top-most protein to mask the activity of the underlying protein. The activity-blocking ability of the top-most protein in cases (4) and (2) in Fig. 2(b) were tested here. Dual-component protein films were immersed in monoclonal antibody specific towards the underlying protein layer. μ CP LN masked $\sim 84\%$ of the underlying FN biological activity relative to the FN positive control (a), whereas μ CP FN masked $\sim 27\%$ of the underlying LN biological activity relative to the LN positive control (b). As a negative control, the cross-reactivity of each mAb toward the micro-contact printed top protein layer was determined to be less than $\sim 1\%$. Bioactivity per surface protein is reported as mean \pm standard deviation ($n = 12$). All outcomes were different at the 95% confidence level ($P < 10^{-4}$).

underlying protein layer is shown in Fig. 7. Our results showed that when LN was μ CP onto a uniformly FN-coated surface, $\sim 84\%$ of the biological activity of the underlying FN was masked by LN. For the reverse patterning order, consisting of μ CP FN onto a uniform LN-coated surface, only $\sim 27\%$ of the biological activity of the underlying LN was masked by FN. As a cross-reactivity control, the activity per protein of each mAb toward the unmatched stamped top protein layer (either μ CP FN or LN) was determined to be less than $\sim 1\%$. The differences in the masking efficiency of the two proteins may be attributed to the structure of the stamped protein on the underlying protein. A closer examination of the μ CP protein topography was conducted by intermittent-contact AFM.

Using featureless (*i.e.*, flat) stamps, FN and LN were separately μ CP onto GMBS-modified substrates to determine the average film thickness and surface texture of μ CP films of each protein following our standard rinsing procedure. Representative AFM images of μ CP FN and LN films are shown in Fig. 8. The average heights of the stamped FN and LN films above the GMBS-modified surface were 6.9 ± 3.6 nm ($n = 206$) and 7.1 ± 2.4 nm ($n = 119$), respectively. The surface topography of stamped FN displayed a highly open texture with many spatial voids, whereas stamped LN appeared to be more uniformly distributed across the surface with fewer spatial voids. As a control experiment, we imaged the surface topography (in both height and phase imaging) of a

featureless (*i.e.*, flat) PDMS stamp before and after incubation in FN for 30 min and the substrate after stamping FN onto a GMBS-modified substrate. The AFM images are shown in Supplemental Fig. 2.⁴⁶ Because of the highly similar topography and structure of the stamp before stamping and the stamped substrate after stamping, the highly open texture of stamped FN is most probably due to the dewetting of the hydrophobic PDMS stamp by the FN solution during the 30 min protein-adsorption period prior to protein stamping onto the GMBS-modified substrates.

Structurally specific antibodies and cell-adhesion assays are useful in determining the structural orientation of immobilized biomolecules.^{49,52} One example is the fluorescence-based ELISA we developed using domain-specific monoclonal antibodies toward FN (A17) and LN (AL-4) active sites known to influence neuronal cell adhesion and neurite outgrowth. We showed that the enzyme turnover activity of HRP on FN and LN was influenced by the protein deposition routes onto GMBS-modified substrates and that each ECM protein behaved differently. Underwood *et al.* measured the structural conformation and biological activity of FN adsorbed on several cell culture-based substrates with the anti-FN (A17) monoclonal antibody.⁵³ Antibody binding was greater on the hydrophilic surfaces (*i.e.*, tissue-culture treated polystyrene) than on hydrophobic surfaces (*i.e.*, untreated polystyrene). Similar results were reported for a fibroblast adhesion assay, where cell adhesion was greatest on the hydrophilic surfaces.

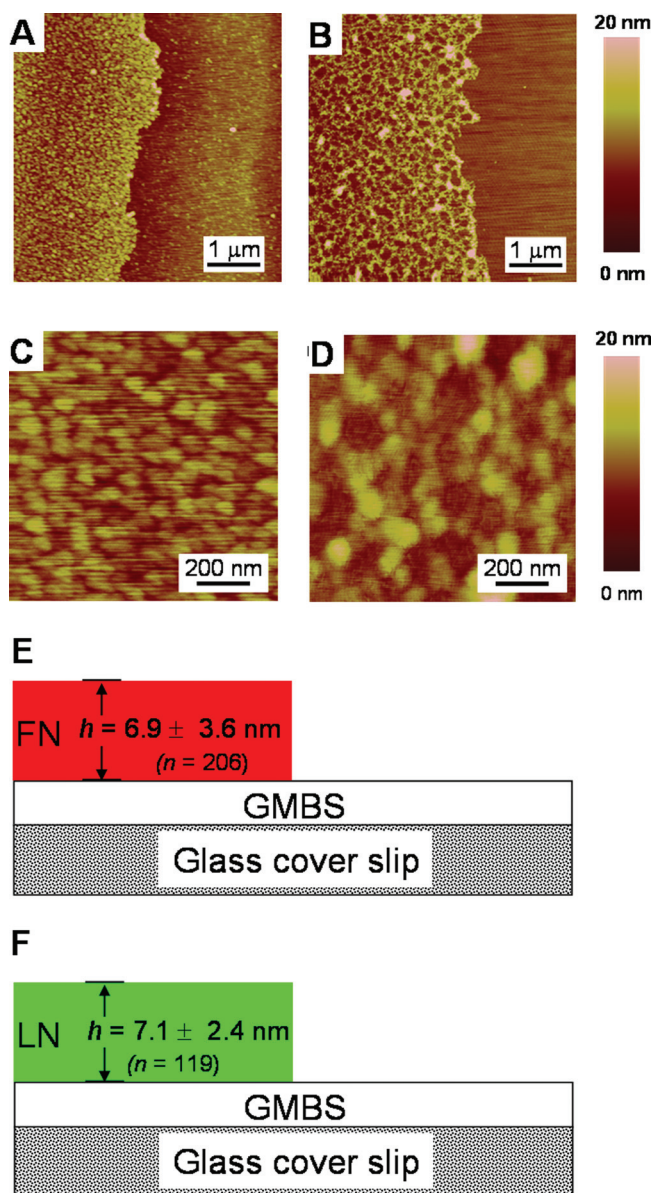


FIG. 8. (Color) Intermittent-contact AFM images of FN and LN deposition onto GMBS-modified substrates by micro-contact printing. PDMS stamps were inked with 50 $\mu\text{g}/\text{ml}$ FN or LN solutions and incubated for 30 min at 4°C. The inked stamps were then brought into conformal contact with the GMBS-modified substrates for 30 min at 37°C with a nominal force of 200 $\text{g}\cdot\text{cm}^{-2}$. The boundaries between the stamped protein regions and the GMBS-modified substrates are shown above for LN (a) and FN (b) with the respective proteins on the left half of the images and the uncontacted GMBS regions on the right half of the images. Higher resolution AFM images obtained entirely within the protein regions highlight the surface texture of the stamped LN (c) and FN (d) regions. The surface texture of μCP LN films (c) displayed a highly open texture with many spatial voids, whereas μCP FN films (d) appeared to be composed of more uniformly distributed proteins with fewer spatial voids. Average film thickness of stamped FN (e) and LN (f). Data reported as means \pm standard deviation.

Although we have only begun to probe the structure of the immobilized ECM proteins on the patterned surfaces (via texture), future experiments will be aimed at using a larger arsenal of monoclonal antibodies and a cell-binding assay using neuronal and glial cells.

AFM analysis of the μCP protein films revealed topographical differences between the two stamped proteins in their surface texture that influenced their ability to serve as a substrate mask. Stamped FN displayed a highly open texture, whereas stamped LN appeared to be more uniformly distributed across the surface with fewer spatial voids. The highly open texture of stamped FN most likely originated from the dewetting of the hydrophobic PDMS stamp by the FN solution during the 30-min stamp-incubation period because the FN adsorption process is entropically favored by the release of bound water molecules.⁵⁴ Similar results were observed by Hodgkinson *et al.* when they attempted to μCP the ECM protein aggrecan, human serum albumin, and laminin.⁴¹ μCP LN and human serum albumin produced relatively smooth films, whereas aggrecan produced a weblike topography. It was noted that during the PDMS stamp-protein incubation period, a significantly larger volume of protein solution was required to wet untreated hydrophobic PDMS stamps (contact angle $\sim 104^\circ$) compared to hydrophilic plasma-treated stamps (contact angle $\sim 16^\circ$). We attempted to perform the protein patterning with plasma-treated stamps, but the transfer of protein from the stamp to the substrate was not reproducible (data not shown). A reasonable explanation is that hydrophobic stamps are able to adsorb more protein molecules during the stamp-protein inking period than hydrophilic stamps.^{31,33,55} These findings suggest that this effect is protein specific.

It is not known what effect the transfer of low-molecular-weight silicone has on the activity of proteins that were patterned by μCP . Nevertheless, transfer is widely known to occur to varying degrees during μCP . A recent study by Thibault *et al.*, identified several key factors when micro-contact printing DNA onto glass and silicon-based substrates.⁵⁶ They were able to reduce the level of silicone transfer by increasing the PDMS curing-time and temperature and minimized the stamp-substrate contact time. They also proposed an aggressive Soxhlet cleaning procedure to extract any low-molecular-weight non-cross-linked silicone fragments from the cured PDMS stamps. Surprisingly, they reported a greater amount of DNA transferred by the uncleaned stamps and suggested that the presence of low-molecular-weight silicone fragments may have a positive influence on the stamping process. Langowski *et al.*, reported a decrease in silicone transfer from plasma-treated PDMS stamps by oxidation of the non-cross-linked oligomers.⁵⁷ Glasmäster *et al.*, reported a similar finding in which they oxidized PDMS stamps by a UV/ozone treatment to significantly reduce silicone transfer.⁵⁸ They also discovered that PDMS stamps with surface texture transferred more silicone-related material than featureless stamps. A more extreme approach was taken by Delamarche *et al.*; in their study, they chemically functionalized the surface of PDMS stamps with PEG-silanes to reduce silicone transfer and increase surface wettability.⁵⁹ Based on these findings, it is evident that progress is being made in identifying the root causes of silicone transfer from the stamp to the substrate during the μCP .

IV. CONCLUSION

This study was part of a larger on-going project aimed at understanding neuronal pathfinding dynamics on patterned

biomaterials using two or more ECM proteins to modulate axonal growth. Allowing the axons to choose between more and less permissive substrates may be a way to control the axon's transition across an unfavorable boundary (e.g., the glial scar), which may be encountered by a regenerating neuron after a spinal cord injury.⁴³

Substrate patterning methods utilizing micro-contact printing techniques and reactive surface chemistry produced well defined lanes of FN and LN with good spatial resolution, good protein contrast, and sufficient interfacial stability. The method of protein deposition (*i.e.*, stamping by μ CP or immobilization from solution) and substrate type (*i.e.*, chemically or biologically modified) significantly affected the biological activity of FN and LN as probed by an ELISA assay. Maximum biological activity per surface protein was achieved by first immobilizing FN from solution, followed by μ CP of LN on the FN. In addition, this route proved favorable for the ability of the topmost protein to mask the protein layer below it. μ CP LN masked ~84% of the underlying FN activity, whereas μ CP FN masked ~27% of the underlying LN activity. Characterization of these substrates by atomic force microscopy revealed similar protein film thicknesses, although stamped FN displayed a highly open texture, whereas stamped LN appeared to be more uniformly distributed across the surface with fewer spatial voids. These results were consistent with the ELISA activity of horseradish peroxidase enzyme in antibody blocking experiments. The sequence of biomolecule deposition required to prepare multiprotein patterned surfaces is often overlooked. To ensure that each protein is properly displayed and not compromised in activity when μ CP is used for patterning, each case must be investigated in detail using surface-sensitive methods and biological assays with careful controls. Based on the limited number of cases studied thus far, it is evident that results will be protein-specific.

- ¹J. C. Harper, R. Polsky, D. R. Wheeler, S. M. Dirk, and S. M. Brozik, *Langmuir* **23**, 8285 (2007).
- ²T. H. Park and M. L. Shuler, *Biotechnol. Prog.* **19**, 243 (2003).
- ³J. V. Veetil and K. M. Ye, *Biotechnol. Prog.* **23**, 517 (2007).
- ⁴J. H. Hyun, H. W. Ma, P. Banerjee, J. Cole, K. Gonsalves, and A. Chilkoti, *Langmuir* **18**, 2975 (2002).
- ⁵S. Mitragotri and J. Lahann, *Nat. Mater.* **8**, 15 (2009).
- ⁶G. MacBeath and S. L. Schreiber, *Science* **289**, 1760 (2000).
- ⁷A. Kaushansky, J. E. Allen, A. Gordus, M. A. Stiffler, E. S. Karp, B. H. Chang, and G. MacBeath, *Nat. Protoc.* **5**, 773 (2010).
- ⁸C. D. Chin, V. Linder, and S. K. Sia, *Lab Chip* **7**, 41 (2007).
- ⁹C. S. Chen, M. Mrksich, S. Huang, G. M. Whitesides, and D. E. Ingber, *Science* **276**, 1425 (1997).
- ¹⁰C. S. Chen, M. Mrksich, S. Huang, G. M. Whitesides, and D. E. Ingber, *Biotechnol. Prog.* **14**, 356 (1998).
- ¹¹M. Mrksich, *Chem. Soc. Rev.* **29**, 267 (2000).
- ¹²D. Lehnert, B. Wehrle-Haller, C. David, U. Weiland, C. Ballestrem, B. A. Imhof, and M. Bastmeyer, *J. Cell Sci.* **117**, 41 (2004).
- ¹³J. A. Hammarback, J. B. McCarthy, S. L. Palm, L. T. Furcht, and P. C. Letourneau, *Dev. Biol.* **126**, 29 (1988).
- ¹⁴Z. P. Zhang, R. Yoo, M. Wells, T. P. Beebe, R. Biran, and P. Tresco, *Biomaterials* **26**, 47 (2005).
- ¹⁵M. L. Condit and P. C. Letourneau, *Nature* **389**, 852 (1997).
- ¹⁶G. M. Whitesides, E. Ostuni, S. Takayama, X. Y. Jiang, and D. E. Ingber, *Annu. Rev. Biomed. Eng.* **3**, 335 (2001).
- ¹⁷G. M. Whitesides, *Nature* **442**, 368 (2006).
- ¹⁸B. A. Langowski and K. E. Uhrich, *Langmuir* **21**, 10509 (2005).

- ¹⁹A. Ohl and K. Schroder, *Surf. Coat. Technol.* **119**, 820 (1999).
- ²⁰B. D. Gates, Q. B. Xu, M. Stewart, D. Ryan, C. G. Willson, and G. M. Whitesides, *Chem. Rev.* **105**, 1171 (2005).
- ²¹Y. N. Xia and G. M. Whitesides, *Annu. Rev. Mater. Sci.* **28**, 153 (1998).
- ²²A. P. Quist, E. Pavlovic, and S. Oscarsson, *Anal. Bioanal. Chem.* **381**, 591 (2005).
- ²³A. Bernard, E. Delamarche, H. Schmid, B. Michel, H. R. Bosshard, and H. Biebuyck, *Langmuir* **14**, 2225 (1998).
- ²⁴H. W. Ma, J. Hyun, Z. P. Zhang, T. P. Beebe, and A. Chilkoti, *Adv. Funct. Mater.* **15**, 529 (2005).
- ²⁵J. Hyun, Y. J.; Zhu, A. Liebmann-Vinson, T. P. Beebe, and A. Chilkoti, *Langmuir* **17**, 6358 (2001).
- ²⁶J. H. Hyun, H. W. Ma, Z. P. Zhang, T. P. Beebe, and A. Chilkoti, *Adv. Mater.* **15**, 576 (2003).
- ²⁷A. Dolatshahi-Pirouz, S. Skeldal, M. B. Hovgaard, T. Jensen, M. Foss, J. Chevallier, and F. Besenbacher, *J. Phys. Chem. C* **113**, 4406 (2009).
- ²⁸G. B. Sigal, M. Mrksich, and G. M. Whitesides, *J. Am. Chem. Soc.* **120**, 3464 (1998).
- ²⁹M. H. Lee, P. Ducheyne, L. Lynch, D. Boettiger, and R. J. Composto, *Biomaterials* **27**, 1907 (2006).
- ³⁰C. F. Wertz and M. M. Santore, *Langmuir* **17**, 3006 (2001).
- ³¹C. F. Wertz and M. M. Santore, *Langmuir* **18**, 706 (2002).
- ³²L. Baugh and V. Vogel, *J. Biomed. Mater. Res.* **69A**, 525 (2004).
- ³³K. E. Michael, V. N. Vernekar, B. G. Keselowsky, J. C. Meredith, R. A. Latour, and A. J. Garcia, *Langmuir* **19**, 8033 (2003).
- ³⁴J. J. Gray, *Curr. Opin. Struct. Biol.* **14**, 110 (2004).
- ³⁵B. Wang, J. Feng, and C. Y. Gao, *Macromol. Biosci.* **5**, 767 (2005).
- ³⁶G. N. Hodgkinson, P. A. Tresco, and V. Hlady, *Biomaterials* **28**, 2590 (2007).
- ³⁷M. Song and K. E. Uhrich, *Ann. Biomed. Eng.* **35**, 1812 (2007).
- ³⁸J. Silver and J. H. Miller, *Nat. Rev. Neurosci.* **5**, 146 (2004).
- ³⁹S. S. G. Johansson, K. Wennerberg, A. Armulik, and L. Lohikangas, *Front. Biosci.* **1**, 126 (1997).
- ⁴⁰S. K. Powell and H. K. Kleinman, *Int. J. Biochem. Cell Biol.* **29**, 401 (1997).
- ⁴¹J. Graf, Y. Iwamoto, M. Sasaki, G. R. Martin, H. K. Kleinman, F. A. Robey, and Y. Yamada, *Cell* **48**, 989 (1987).
- ⁴²Y. Iwamoto, F. A. Robey, J. Graf, M. Sasaki, H. K. Kleinman, Y. Yamada, and G. R. Martin, *Science* **238**, 1132 (1987).
- ⁴³K. Tashiro, G. C. Sephel, B. Weeks, M. Sasaki, G. R. Martin, H. K. Kleinman, and Y. Yamada, *J. Biol. Chem.* **264**, 16174 (1989).
- ⁴⁴M. Q. Zhang and M. Ferrari, *Biotechnol. Bioeng.* **56**, 618 (1997).
- ⁴⁵M. Q. Zhang and M. Ferrari, NCBI, National Center for Biotechnology Information (NCBI), In National Library of Medicine.
- ⁴⁶M. Q. Zhang and M. Ferrari, See supplementary material at E-JCPSA6-6-304103 for XPS analysis of mono- and dual-component protein films used for the ELISA bioassay and tapping-mode AFM images of PDMS stamps before, during, and after protein incubation and micro-contact printing of fibronectin.
- ⁴⁷P. S. Hale, P. Kappen, W. Prissanaroon, N. Brack, P. J. Pigram, and J. Liesegang, *Appl. Surf. Sci.* **253**, 3746 (2007).
- ⁴⁸Y. S. Lo, N. D. Huefner, W. S. Chan, P. Dryden, B. Hagenhoff, and T. P. Beebe, *Langmuir* **15**, 6522 (1999).
- ⁴⁹P. A. Underwood, J. G. Steele, and B. A. Dalton, *J. Cell Sci.* **104**, 793 (1993).
- ⁵⁰S. Scheele, T. Sasaki, A. Arnal-Estape, M. Durbeek, and P. Ekblom, *Matrix Biol.* **25**, 301 (2006).
- ⁵¹U. M. Wewer, G. Tarabozetti, M. E. Sobel, R. Albrechtsen, and L. A. Liotta, *Cancer Res.* **47**, 5691 (1987).
- ⁵²A. J. Garcia, P. Ducheyne, and D. Boettiger, *Biomaterials* **18**, 1091 (1997).
- ⁵³P. A. Underwood, J. G. Steele, and B. A. Dalton, *J. Cell Sci.* **104**, 793 (1993).
- ⁵⁴G. K. Toworfe, R. J. Composto, C. S. Adams, I. M. Shapiro, and P. Ducheyne, *J. Biomed. Mater. Res. A* **71A**, 449 (2004).
- ⁵⁵L. Vroman, *Nature* **196**, 476 (1962).
- ⁵⁶C. Thibault, C. Severac, A. F. Mingotaud, C. Vieu, and M. Mauzac, *Langmuir* **23**, 10706 (2007).
- ⁵⁷B. A. Langowski and K. E. Uhrich, *Langmuir* **21**, 6366 (2005).
- ⁵⁸K. Glasmäster, J. Gold, A.-S. Andersson, D. S. Sutherland, and B. Kasemo, *Langmuir* **19**, 5475 (2003).
- ⁵⁹E. Delamarche, M. Geissler, A. Bernard, H. Wolf, B. Michel, J. Hilborn, and C. Donzel, *Adv. Mater.* **13**, 1164 (2001).